J MATER SCI 41 (2006) 485–504

Fabrication of CuSiC metal matrix composites

GLENN SUNDBERG*
Department of Chemical and Nuclear Engineering, Center for Advanced Materials, University of Massachusetts, Lowell; Department of Engineering Technology, University of Massachusetts, Lowell
E-mail: glenn_sundberg@uml.edu

PRADEEP PAUL, CHANGMO SUNG, THOMAS VASILOS
Department of Chemical and Nuclear Engineering, Center for Advanced Materials, University of Massachusetts, Lowell

Published online: 17 January 2006

A CuSiC MMC heatspreader will offer high thermal conductivity between 250 and 325 W/mK and corresponding adjustable thermal expansion coefficient between 8.0 and 12.5 ppm/°C. The primary challenge of CuSiC manufacture was to prevent reaction between copper and silicon carbide during high temperature densification, which dramatically degraded the thermal conductivity. In this study, the key issue addressed was the Si attack of Cu at the temperatures necessary for CuSiC fabrication (850 to 1200°C). Decomposition of SiC in contact with copper will dissolve Si in Cu causing a dramatic decrease of Cu thermal conductivity. This diffusion of Si into Cu can be prevented by the application of reliable barrier layers to diminish mass transport through the diffusion path and thereby minimizing the chemical interaction. A reliable barrier coating was identified and used to fabricate the CuSiC composites. The CuSiC composites were then characterized by SEM, TEM, XRD and XPS. Chemical analysis and thermal conductivity by laser flash diffusivity measurement illustrated the effectiveness of the barriers. A CuSiC composite having thermal conductivity of 322.9 W/m-K was successfully fabricated.

1. Introduction

High power electronics require novel thermal management materials for heatsinks and heat spreaders with both high thermal conductivity and an adjustable coefficient of thermal expansion. The high heat transfer necessary for higher power density is easily obtained from traditional high thermal conductivity metals, such as copper, but reliability of large form factor, high power modules can suffer from coefficient of thermal expansion (CTE) mismatch with the Cu baseplate. The purest copper materials have a 397 W/mK thermal conductivity, but unfortunately a CTE as high as 15.9 ppm/°C creates issues with expansion mismatch stress during thermal transients in assembly and service. Practical thermal management materials with lower coefficient of thermal expansion than copper typically have a lower thermal conductivity than copper. Adjustable thermal expansion coefficient MMC materials, such as AlSiC, have been accepted as heat spreaders for converters used in large electronic drives for trains, but thermal conductivity is approximately half that of copper [1].

This paper discusses the development of a copper-silicon carbide (CuSiC) metal matrix composite (MMC). A CuSiC MMC heatspreader will offer higher thermal conductivity between 250 and 325 W/mK and corresponding adjustable thermal expansion coefficients between 8.0 and 12.5 ppm/°C. CuSiC will be compatible with industry standard CuAg eutectic brazing (CuSil) at ~800°C, water based cooling systems (vapor chambers, heat pipes, cold-plates) and will allow integration of high thermal conductivity materials, such as diamond and highly oriented pyrolytic graphite (PG) into the CuSiC structure), to maximize heat spreading (*x*-*y* direction) and/or through (*z*-direction) heat transfer. Most importantly, alone or with

*Author to whom all correspondence should be addressed.
0022-2461
DOI: 10.1007/s10853-005-2622-3

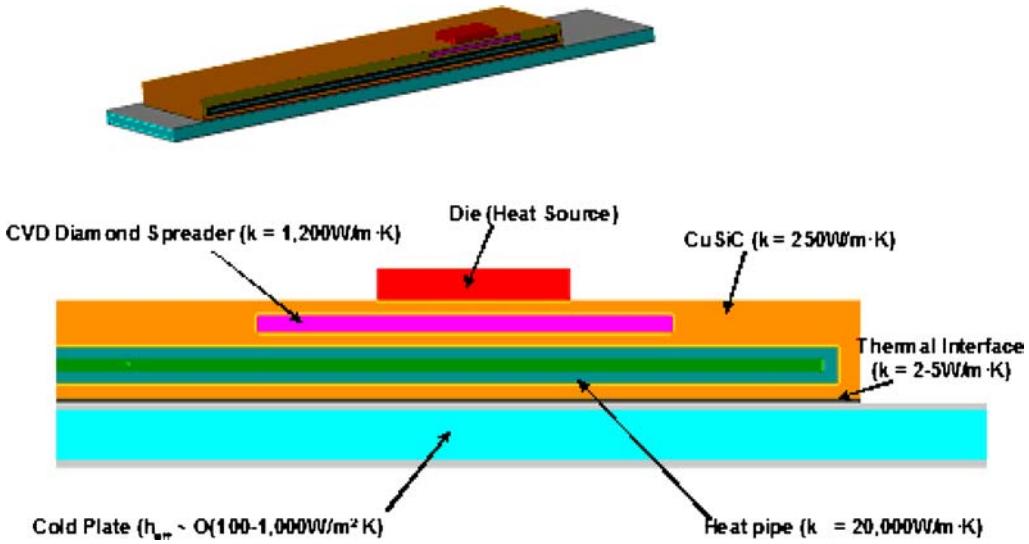

Figure 1 CuSiC heat pipe with integrated diamond heat spreader.

integrated high k materials, the CuSiC can be used to manufacture water based heat pipes, vapor chambers and cold-plates (Fig. 1) to achieve +25,000 W/mK effective thermal conductivity [2].

The main challenge is that Cu chemically reacts with SiC at temperatures necessary for CuSiC fabrication (850 to 1200°C). The decomposition of SiC in contact with Cu at elevated temperature dissolves Si into Cu with an expected concomitant decrease of Cu thermal conductivity [3]. The solubility of Si in Cu is about 5% at 850°C [4]. The affinity of Cu for C is negligible (the solubility of C in Cu at 1150°C is in the ppm range and the contact angle of Cu on graphite is 120° or greater). However, Cu and Si develop strong interactions as indicated by the presence of several Cu-Si compounds in the copper-silicon phase diagram [5]. Small amounts of Si dissolved in Cu can degrade thermal properties as illustrated by C65100 low silicon bronze (98.5% Cu–1.5%Si) with a thermal conductivity of 57 W/mK as compared to C10100: oxygen-free, high purity electronic copper with a thermal conductivity of 391 W/mK [6].

The key to achieving a useful CuSiC material is control of the reaction between SiC and Cu. Two approaches were investigated to control SiC reaction with Cu. First, passivation coatings were evaluated upon SiC as a barrier to Cu diffusion. Secondly, the thermal exposure of SiC and Cu was minimized during consolidation using high pressure forging with a short cycle time.

1.1. Particle distribution measurements of CuSiC composites

In order to determine the microstructure-property relationships of the composites, a methodology for a quantitative description of the structure was required. For example, Lewandowski *et al.* [7] studied the relation between particle size and spatial distribution characteristics on the accumulation of damage leading to fracture by using the Dirichlet tessellation method. In the present scenario, a methodology to quantify the uniformity of the SiC distribution in the Cu matrix was needed. The particle distribution was very important since it was directly related to the thermal conductivity, k of the composite. In the past there were a number of methods applied, these include the average interparticle spacing or mean free path [8], the nearest and near neighbor distances [9, 10], the local area fraction [9], the average number of particles contained within an imaginary test sphere of given size [11], the radial distribution function [11], and local energy dispersive X-ray analysis techniques [12]. Of the preceding techniques the four most common techniques are [12, 13].

- Mean free path between particles;
- Nearest-neighbor particle centers of gravity distance;
- Quadrat method for local particles concentration;
- Radial distribution function.

An analysis of each of these methods was performed to select a method to assess the degree of uniformity of the SiC particles in the Cu matrix.

1.1.1. Mean free path

In this technique the mean free path, d_p [14] is calculated from the volume fraction of particles, V_f, and the sum of the perimeter length, P_p, of all particles in a total test area, At [15]:

$$d_p = (\pi(1 - V_f)A_t)/P_p \quad (1)$$

According to Equation 1, d_p represents the average distance from one SiC particle to all the other SiC particles. The main disadvantage of this technique was that it introduced a degree of uncertainty by the identification of a cluster of very small particles as an individual particle. Consequently, the measured perimeter length could be falsely determined to be less than actual, resulting in a falsely high d_p value.

1.1.2. Nearest neighbor distance

The nearest neighbor distance function $d(r)$ is defined as the distance between the centroids of the nearest neighboring particles [12, 16, 17]. This technique again had shortcomings in systems wherein particles were grouped together in groups of two or more. The resulting nearest neighbor distance approximated the diameter of the individual particle giving a false low $d(r)$ value.

1.1.3. Radial distribution function

Radial distribution function $K(r)$ is defined by the relation of the number of particles, N_{ra} lying at a distance not bigger than r (the distance from the point of reference and the area of circle with radius r) divided by N_a, the mean number of particles per unit area over the whole sample [18]

$$K(r) = N_{ra}/N_a \tag{2}$$

Fig. 2 shows a schematic representation of the radial distribution function methodology. N_{ra} is the number of particles lying with the area of circle with radius r. The point of reference is grey and the counted particles associated with N_{ra} are black. A uniformly distributed microstructure would have a $K(r) = 1$ for any circle radius. A clustered distribution however has a sharp peak at small r values, rapidly dropping to a plateau of approximately 1 at larger r values. The radial distribution function method was an accurate method but was time consuming and tedious in comparison to the quadrat method.

1.1.4. Quadrat method

In the quadrat method [19], a microstructure image is divided into a grid of square cells and the number of particles in each cell, N_q, is determined. An ordered particle distribution would generate a large number of quadrats containing approximately the same number of particles. On the other hand, a distribution with clusters of closely spaced particles would be expected to produce a combination of empty quadrats, quadrats with a small number of particles, and quadrats with many particles. A random distribution would produce results somewhere in between these two extremes.

The quadrat method has some ambiguity with determination of the optimal quadrat size. Deviations from random distribution are highly dependent on the size and shape of the sample quadrat [19]. A very small sampling quadrat will detect many particle-free areas, falsely indicating clustering, whereas a very large quadrat will tend to give the same number of particles in each quadrat, regardless of clustering effects. The optimum quadrat size can be found by physical analysis of the microstructure, which may suggest some interaction range between particles, or simply by a trial-and-error method [20]. Other methods of determining the optimum quadrat size also have been suggested [19, 21, 22]. A simple but effective rule used in this study was that the optimum square quadrat size should be approximately twice the size of the mean area per particle [22].

Bias introduced by edge effects was minimized by counting the total number of particles completely inside each quadrat and those in contact with the left and bottom quadrat sides. In this manner, particles on the quadrat edge were not counted more than once (Fig. 3). Study of the MMC microstructures shows that the overall shape of the N_q distribution varied significantly with the degree of clustering. Indeed, increasing the size of SiC clusters caused the observed N_q distribution to become less symmetric. The degree of asymmetry of a statistical distribution around the mean can be quantified by its skewness ß, which is defined by Equation 3 [3].

$$\beta = (q/((q-1)(q-2)))\Sigma\left(\left(N_{qi} - N_q^{mean}\right)/\sigma\right)^3 \tag{3}$$

Where q is the total number of quadrats studied, N_{qi}; is the number of SiC particles in the ith quadrat ($i = 1, 2 \ldots q$), N_q^{mean} is the mean number of SiC particles

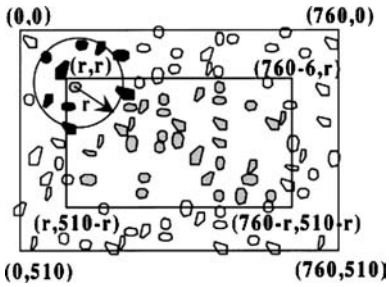

Figure 2 Schematic representation of the method used to determine the radial distribution function. Particles identified as circle centers are denoted in grey and counted particles in black. The outer frame size is 760 × 510 pixels, the disc has a radius r, and all dimensions are in pixels [13].

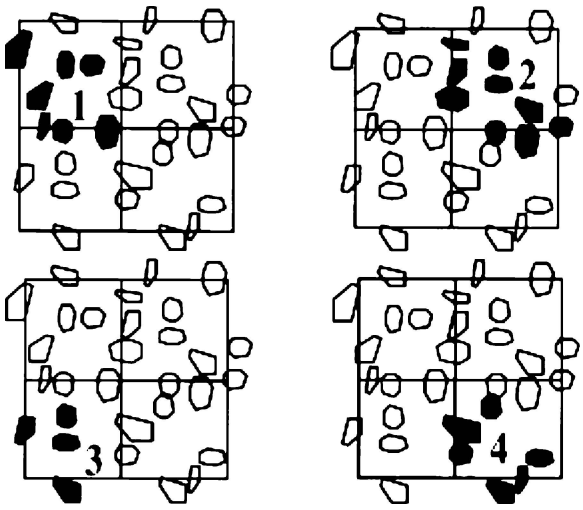

Figure 3 Schematic representation of the quadrat method, using four quadrats. Counted particles are denoted in black [13].

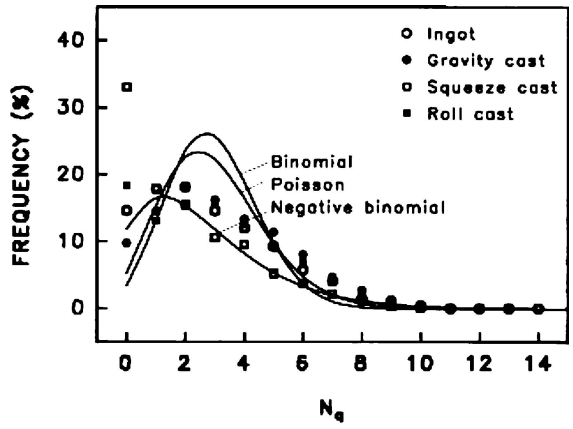

Figure 4 Theoretical distribution curves and experimental results (symbols) from the quadrat analysis from A356/10% SiC [13].

per quadrat, and s is the standard deviation of the N_q distribution. An increase in ß indicates an increase in the prevalence of SiC clustering.

The quadrat method very effectively detected variation of SiC particle distribution in MMCs induced by processing. The results from the quadrat analysis can also be compared with theoretical regular, random, or clustered distributions defined by exact statistical relation. Such a comparison can be useful in optimizing the dispersion of reinforcing particles in a MMC.

Random, regular, and distributions of particles as clusters can be expressed in mathematical terms if the particles are assumed to be points (i.e., their cross-sectional areas are zero). As shown in Fig. 4, it has been proven mathematically [13] that a random spatial distribution of points follows the Poisson model, a regular spatial distribution the binomial model, and a clustered spatial distribution the negative binomial model [13]. The quadrat method and the radial distribution function were the most accurate of the above stated techniques to determine the uniformity of the SiC distribution. The quadrat method was chosen since it was less time consuming than the radial distribution function.

TABLE I Characteristics of the SiC powders obtained from vendors

SiC	Description	Size (mesh)	Oxidation protection	Total impurities	Oxygen
Uncoated					
A	Acid Wash	240	No	<1 wt%	0.029 wt%
Cu/TiN Coated					
Bl	25 vol% Cu	240	Yes	<0.20 wt%	0.590 wt%
B2	30 vol% Cu	240	Yes	<0.14 wt%	0.681 wt%
B3	30 vol% Cu	240	No		
Cu Coated					
Cl	69 vol% Cu	325	No		
C2	35 vol% Cu	325	No		
C3	70 vol% Cu	325	No		
Cu Uncoated					
Dl		−170+400	No	<0.05 wt%	0.048 wt%
D2		−325	Yes	<0.11 wt%	0.122 wt%

2. Experimental procedure

2.1. SiC powders

SiC powders were obtained from several vendors. Four types of SiC powders were used in this study: bare, Cu/TiN coated, Cu coated and Cu blended with SiC powders with which various formulations were pressure densified (Table I). The Cu/TiN coated SiC powders used for hot pressing had oxidation protection in the form of thin organic coatings applied after the Cu coating. The nominal sizes (average size of the SiC particle) were 240 and 325 mesh with total impurities less than 1 wt%.

2.2. Hot pressing of coated SiC powders

Hot pressing of blended CuSiC powders was performed in a square, 1.3 × 1.3 in, graphite mold with two movable rectangular graphite plungers used to apply pressure to the powders. The hot press furnace used graphite resistance heating elements to heat at an average

TABLE II Compositions used in hot pressed composites and hot pressing conditions

Hot press ID	Description	Conditions
HA	50 vol% Cu(Dl): 50 vol% SiC (A)	1065°C for 40 min at 7.7 ksi
HB	50 vol% Cu (Dl)-50 vol% SiC(A)	965°C for 40 min at 7.7 ksi
HC	50 vol% Cu (Dl):50 vol% SiC (A)	865°C for 40 min at 7.7 ksi
HD	50 vol% Cu (D2): 50 vol%Cu/ TiN coated SiC (Bl)	910°C for 40 min at 7.7 ksi
HE	50 vol%Cu(D2):50 vol% Cu/TiN coated SiC (B2)	Upset forging at 25,000 1b
HF	50 vol% Cu (D2):50 vol% Cu/TiN coated SiC (Bl)	1065°C for 40 min at 7.7 ksi

TABLE III Compositions used in the forging of CuSiC composites

Forge Ids	Description
FA	50 vol% Cu: 50 vol% SiC: Cu/TiN coated SiC (Bl) blended with Cu (D2)
FB	50 vol% Cu:50 vol% SiC: Cu/TiN coated SiC (B2) blended with Cu (Dl)
FC	50 vol% Cu:50 vol% SiC: Cu/TiN coated SiC (B2) blended with Cu (D2)
FD	69 vol% Cu:31 vol% SiC (Cl) No blending
FE	50 vol% Cu: 50 vol% SiC: Uncoated SiC (A) blended with Cu (Dl)
FF	70 vol% Cu: 30 vol%SiC (C3) No blending
FG	41 vol% SiC-59 vol%Cu (C2) No blending

TABLE IV CuSiC composites used to quantify uniformity of SiC grain distribution uniformity

Sample	Description
FB	50 vol% Cu: 50 vol% SiC: Cu/TiN coated SiC (B2) blended with Cu (Dl)
FD	60 vol% Cu: 40 vol% SiC: No blending
FF	70 vol% Cu: 30 vol%SiC (C3) No blending
FC	50 vol% Cu:50 vol% SiC: Cu/TiN coated SiC (B2) blended with Cu (D2)

rate of 12°C/min from ambient to the maximum soak temperature. Temperature was measured with an optical pyrometer sighted upon the graphite mold during hot pressing. The retort surrounding the furnace was a water cooled cold-wall chamber that was evacuated to a vacuum of ∼200 μm of mercury prior to applying power to the heating elements. Two hydraulic cylinders, mounted on the upper and lower horizontal section of the press frame, applied force to two water cooled ram extensions that passed through sliding vacuum seals at the top and bottom of the chamber. The ram extensions exerted a load upon the plungers of the graphite mold to pressure densify the loose CuSiC powder inside. Pressure was gradually increased during heating to the desired maximum pressure approximately 30 min before the maximum soak temperature was reached. The cooling rate averaged 5.5°C/min from soak temperature to 865°C. Below 865°C there was insufficient radiant energy to record temperature with

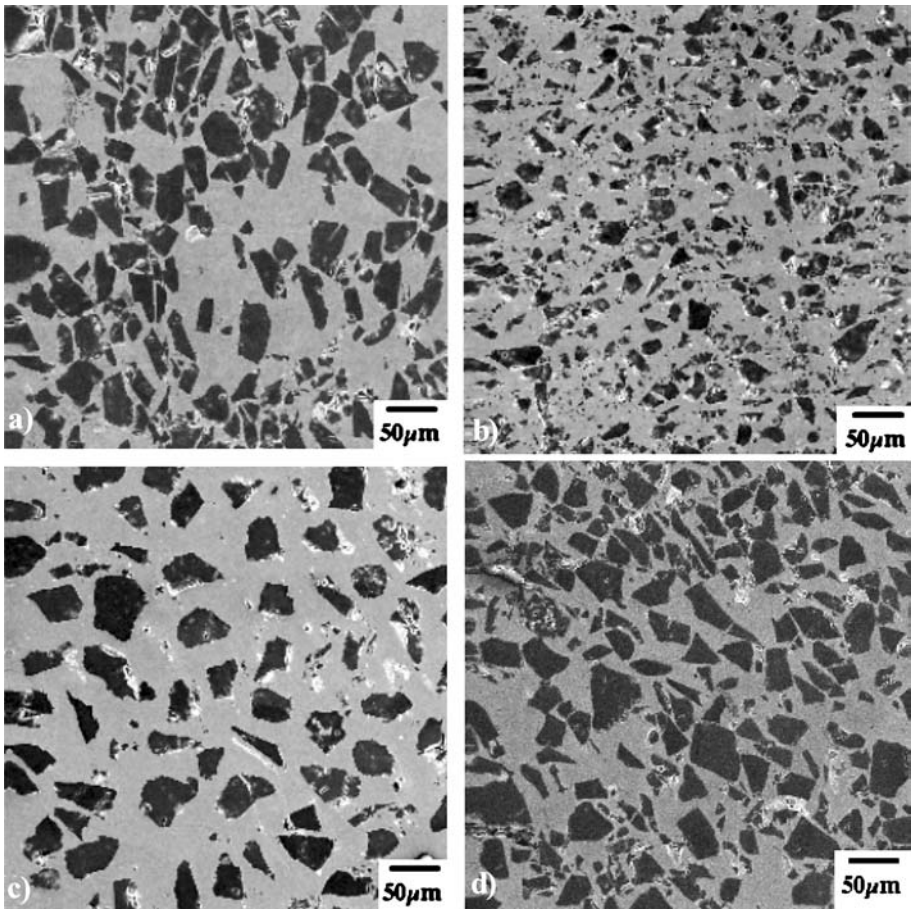

Figure 5 SEM micrographs of samples: (a) FB (part blending), (b) FD (no blending), (c) FF (no blending), and (d) FC (blending).

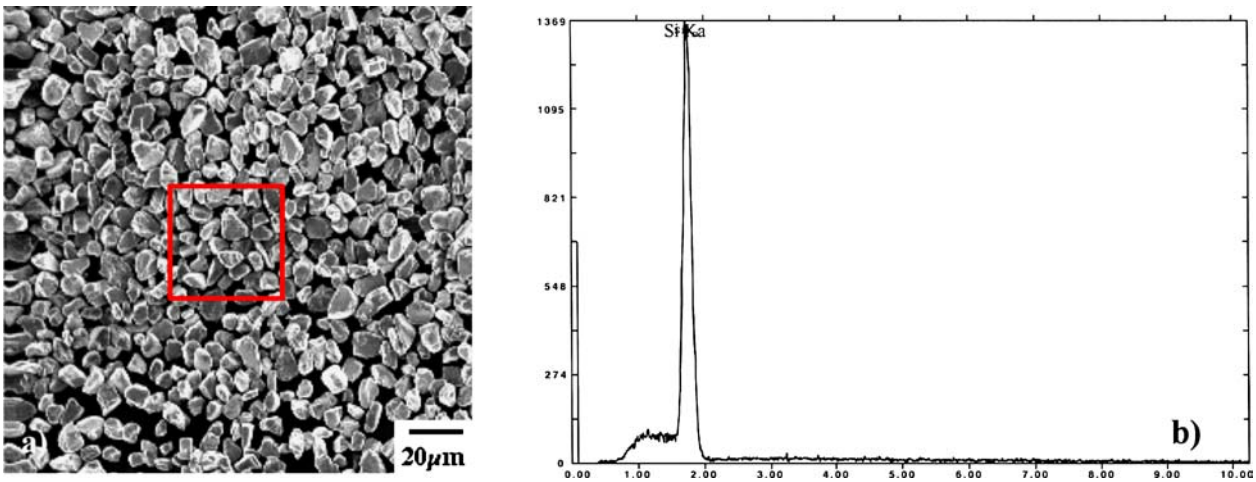

Figure 6 (a) SEM image of the uncoated sample A. (b) EDX spectrum of the uncoated sample A.

the optical pyrometer. Movement of the upper ram was monitored by a linear variable displacement transformer that reported ram movement to within ±0.001 in.

Sample Bl SiC powder used for hot pressing was nominally 19 vol% Cu: 8l vol% SiC with a ∼70 nm thick TiN barrier coating applied directly on the SiC grain with a Cu overlayer deposited above the TiN barrier. Only the Cu component will plastically deform during pressure densification with sufficient applied pressure and temperature. If the contact stress between adjacent SiC grains during pressure densification is greater than the plastic yield stress of the Cu, then the Cu will extrude between SiC

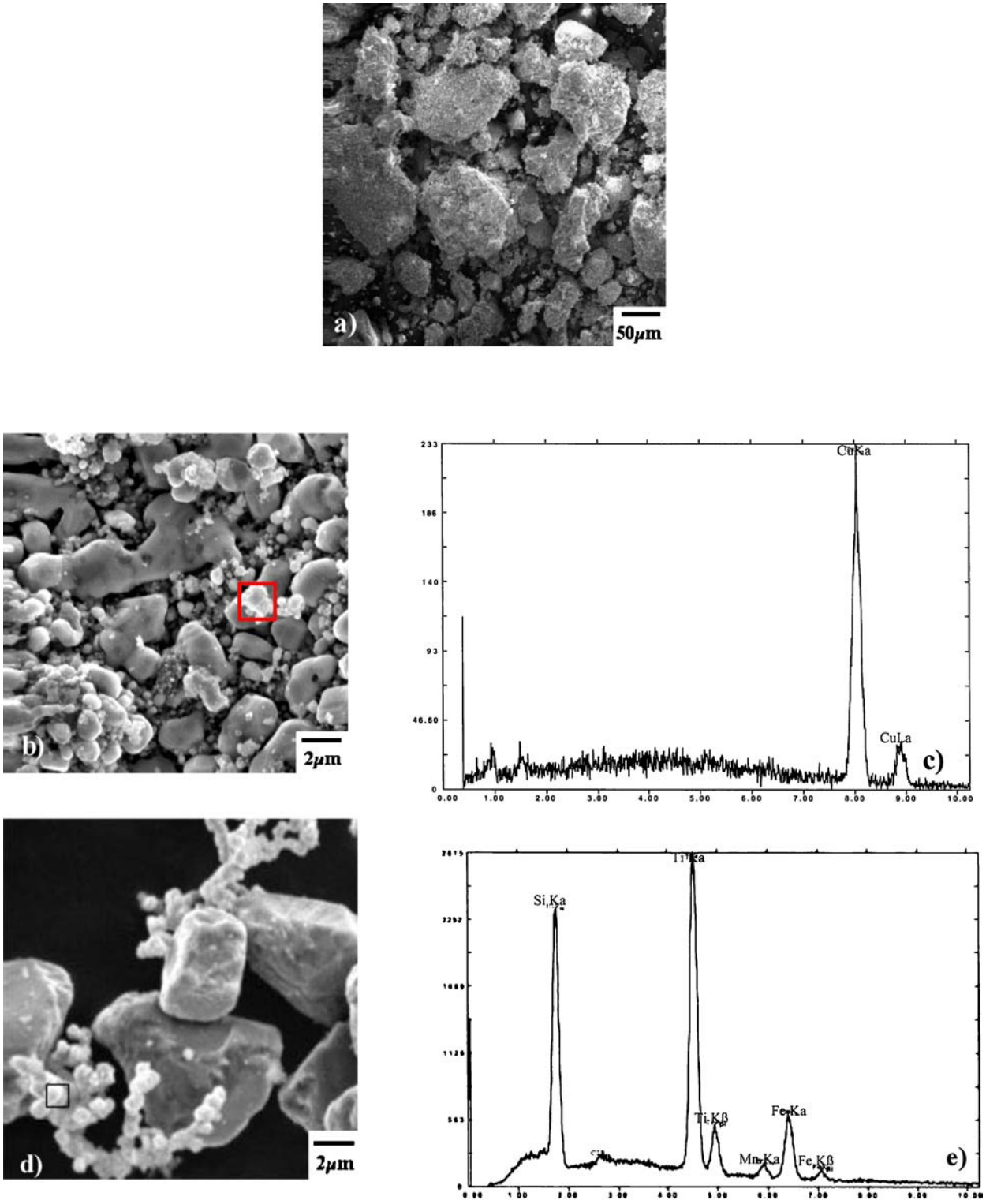

Figure 7 SEM/EDX of poorly coated SiC powder (Sample B3): (a) SEM image of SiC grain with loosely bound Cu coating, (b) SEM image at 5000 × magnification showing soots of the coating, (d) image demonstrating partial coverage, contamination and TiN poorly adherent "soot", (c) and (e) EDX spectra.

grains to fill porosity. The SiC component will not soften and flow during pressure densification.

The uncoated SiC powder A alone was estimated to achieve a maximum packing density of 60 to 65% of theoretical density, with 35 to 40 vol% porosity between the SiC grains, prior to application of pressure and temperature. The Cu/TiN coated SiC powders (Bl and B2) were nominally 75 vol%SiC: 25 vol%Cu after fluidized bed CVD coating. The amount of Cu on the coated SiC powder was not sufficient to fill the void space between the SiC grains to obtain a fully dense body after hot pressing. Additional Cu was dry blended into the Cu/TiN coated SiC

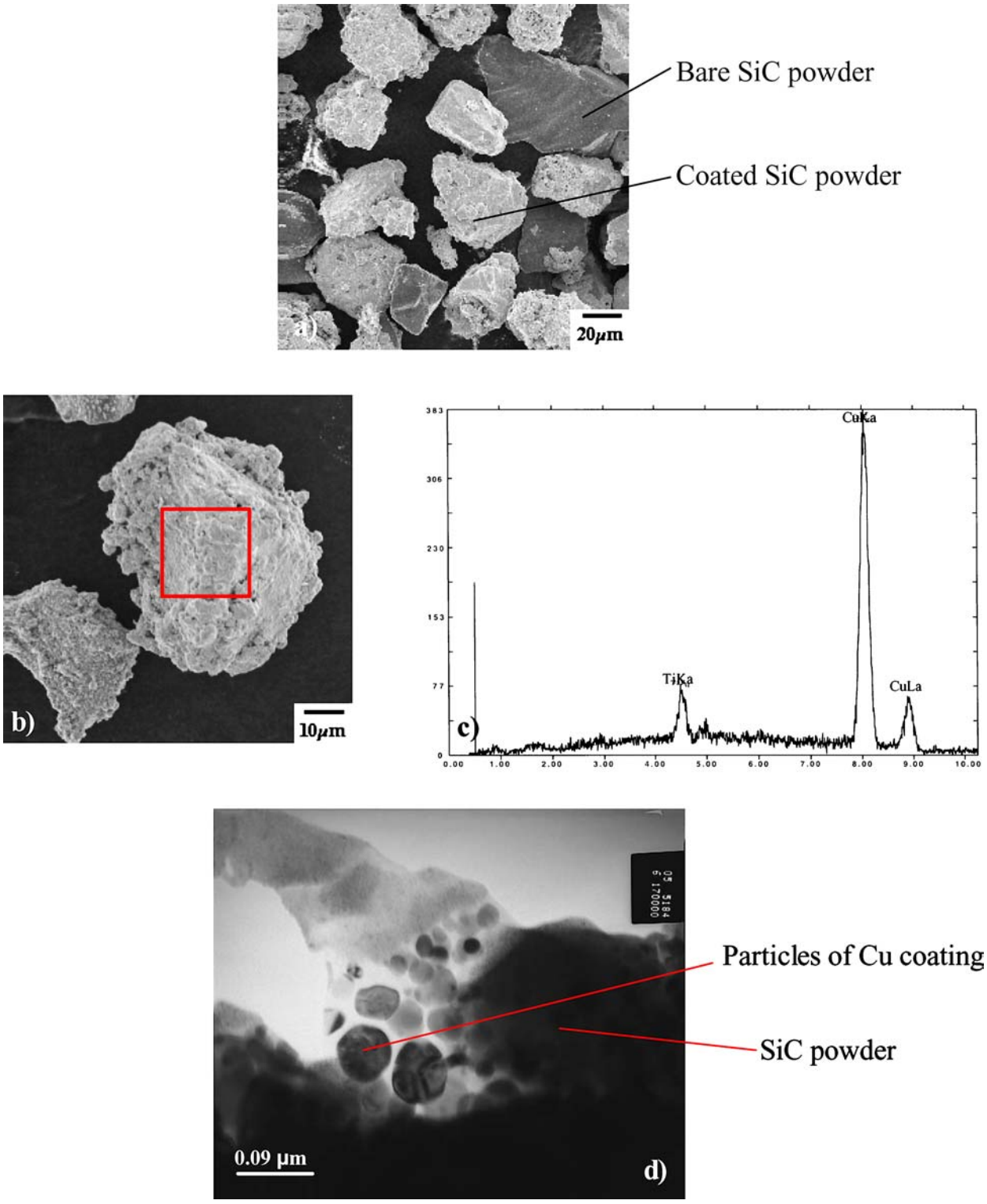

Figure 8 Improved coated SiC powder with TiN barrier and Cu overlayer Sample Bl: (a) and (b) SEM images, (c) EDX Spectrum indicating the Cu peaks with the TiN underlayer, (d) TEM image of the SiC powder with removed Cu coating grains.

powder prior to hot pressing to provide sufficient Cu to fill all of the intergranular pores after hot pressing and achieve a fully dense body with no porosity. Small amounts of residual porosity were not desired since this will serve to impede heat transfer resulting in decreased thermal conductivity. Table II gives the compositions of the powders used during hot pressing. Sample HD was blended powder of nominal composition 50 vol% Cu-50 vol%SiC made from the sample Bl powder blended with sample Dl powder. 25.3 gm of this powder was placed in a graphite die of dimensions 1.3 × 1.3 in and was hot pressed to 7.7 ksi at soak of 910°C for 40 min.

Sample HE was blended powder of nominal composition 50 vol% Cu-50vol%SiC made from the sample B2 Cu/TiN coated SiC blended with Cu sample D2. 50.1 g of the powder was cold pressed in a steel die first into a compact at l0 ksi to make a compact of dimensions 1.254 in diameter × 0.711 in tall. This was then forged between two 4 inch diameter platens without a closed die to maximum load of 25000 1b. This is termed "upset forging". The CuSiC diameter increased significantly until the CuSiC body was the size of the platens so it was difficult to tell the exact pressure the part experienced during forging. The upset forging average soak temperature was 863°C and the time at pressure was 12 min. The load was increased from 10,000 1b at start of soak to 20,000 1b at 2 min into the soak and finally it was increased to 25,0001b at 7 min into soak. The load was removed and ram raised after the 12 min soak. This upset forging was not successful to eliminate porosity, the CuSiC body was not dense after forging.

2.3. Forging of coated SiC powders

Powders were cold pressed into a 2 inch diameter coupon at 33 ksi. The coupon was pre-heated prior to forging by placement in a furnace pre-heated to 850°C in a reducing atmosphere. After 10 min the 850°C coupon was transferred to the forge for pressure densification at 50 ksi in a reducing environment. Forging at 50 ksi takes place in 15 s. The forged coupon exited the forge in less than a minute at ∼250°C after which it

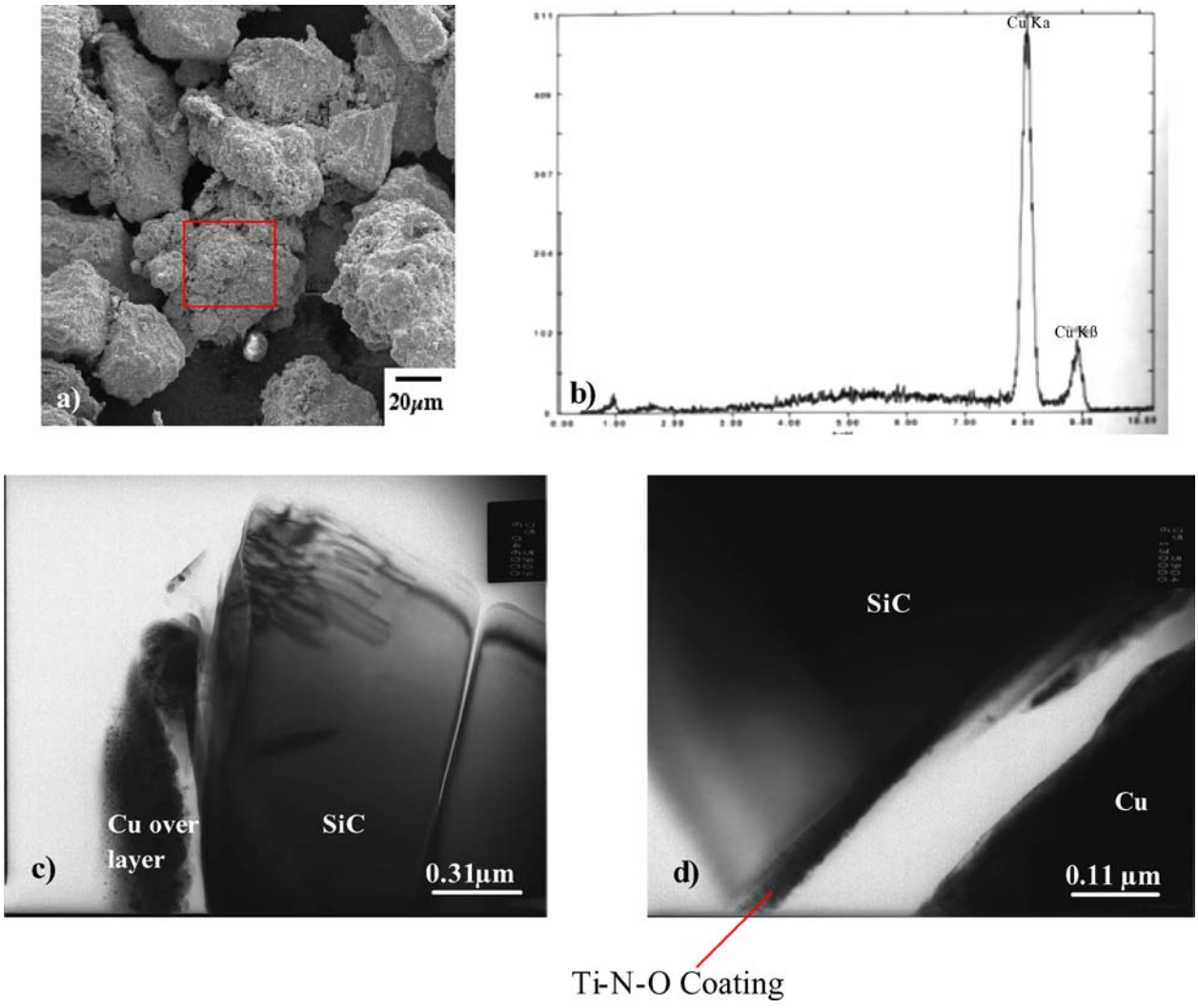

Figure 9 Coated SiC powder with TiN barrier and Cu overlayer Sample B2: (a) SEM image of coated SiC grains, (b) EDX spectrum showing only the Cu overlayer, (c) and (d) TEM images of the coated SiC powders showing the Cu overlayer and the Ti–N–O coating layer.

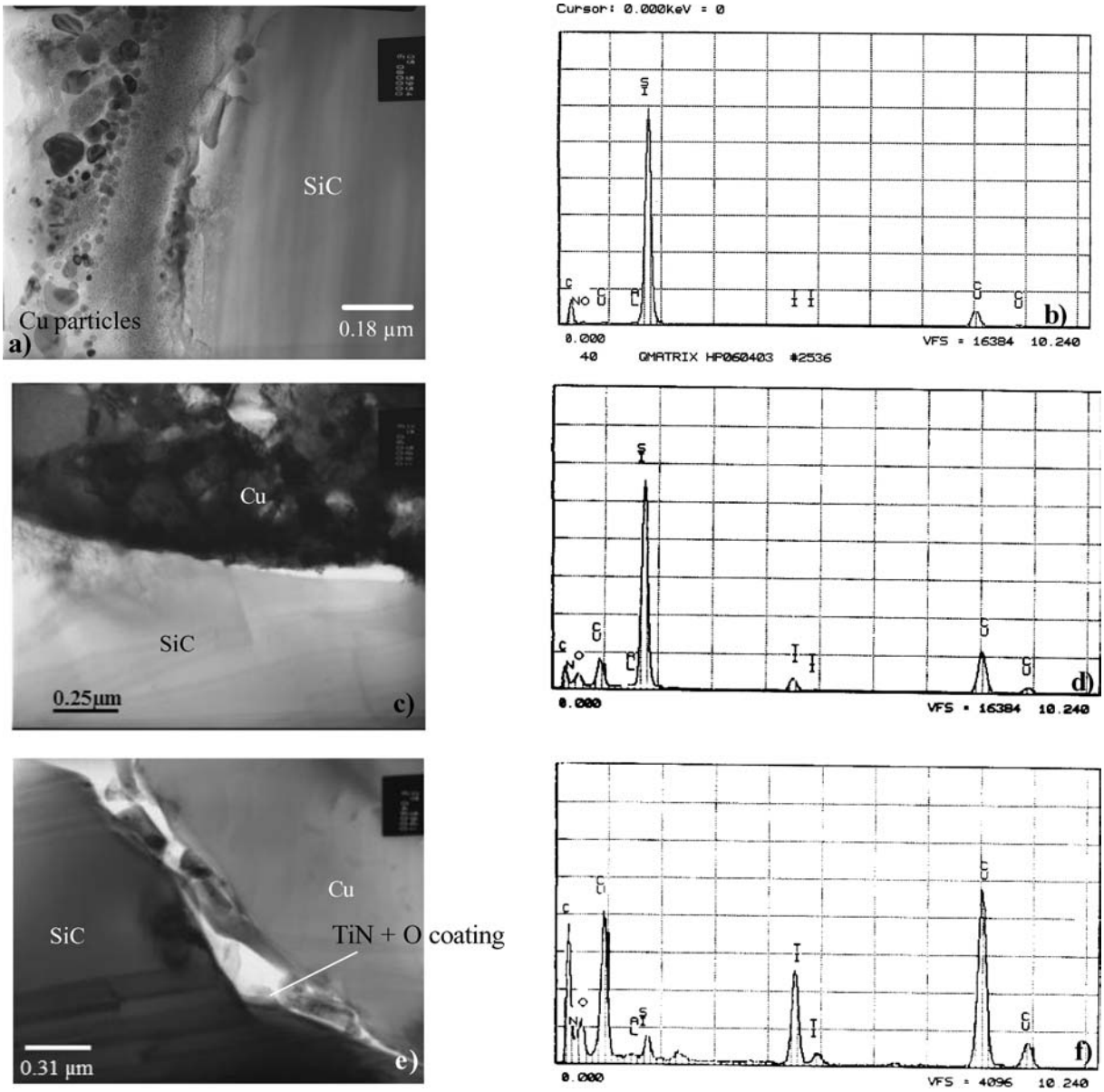

Figure 10 Sample HF: (a) and (b) TEM image showing no Ti coating at the interface with corresponding EDX spectra; (c) and (d) TEM image showing a thin layer of Ti in corresponding EDX spectra; (e) and (f) TEM image depicting a TiN + O coating in corresponding EDX Spectra.

was air-cooled. The raw materials used for the forging are given in Table I. The description of the samples used in forging study are given in Table III.

2.4. Statistical methods to quantify the uniformity of the SiC distribution

In this section, statistical methods were used to determine the uniformity of the SiC distribution in the Cu matrix. This was done to evaluate the relationship between SiC particle distribution and physical properties such as density and thermal conductivity. The samples used to quantify the uniformity of the particle distribution were sample FD (see Table IV and Fig. 5b), sample FB (Fig. 5a), sample FF (Fig. 5c) and sample FC (Fig. 5d). Samples FD and FF were processed with no blending of the Cu and SiC powders, instead all of the Cu was directly applied as a coating deposited onto the SiC grains before forging. Samples FB and FC were processed with the blending of the Cu and Cu coated SiC powders.

The quadrat method was used to quantify uniformity of the SiC grain distribution. All images used for analysis were taken using an AMRAY 4000 SEM at 20 kV and l00× magnification. In the quadrat method the image processing was done using Adobe® Photoshop® ver. 7. The area of interest (AOI) was first selected and thresholding was done to obtain a high contrast image. A 9 × 9 cm hard copy of the threshold image was then printed. By trial and error, the optimum size of the quadrat was determined to be a 1 cm by 1 cm square grid. A template consisting of the accurately measured grids was drawn onto a transparent sheet. The sheet was then superimposed onto the image, the individual particles in the grids were counted and the frequency versus N_q plot was drawn.

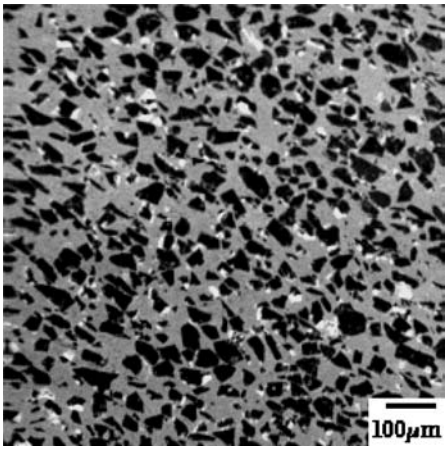

Figure 11 SEM image of Sample HE showing the angular morphology of the SiC grains indicating no reaction.

3. Results and discussion

3.1. Hot pressing of CuSiC metal matrix composites

3.1.1. Characterization of SiC powders

Bare SiC powders (sample A) prior to coating samples Bl, B2 and B3 were characterized using the scanning electron microscope (SEM) with the energy dispersive X-ray spectrum (EDS). Fig. 6a and b shows SEM/EDS analysis of uncoated SiC powder A. The rectangular box in the image indicates the area of EDS analysis. The SEM/EDS analysis shows a narrow size distribution (~5–l0 μm) of the angular SiC powders and the absence of impurities. Impurities were a concern since they can be detrimental to the thermal conductivity of the composites. Initially a sample Cu/TiN coated powder (B3) was characterized for quality assurance from the vendors. The coatings had poor adherence to the SiC substrate. Bare SiC grains were observed with partially coated surfaces. Contamination with Fe, Cl and Mn was detected by SEM (Fig. 7e). Ti concentration on SiC was highly variable. Much of the Ti was associated with poorly adherent, homogeneously nucleated Ti rich "soots" (Fig. 7d). Consequently, this powder was not used for hot pressing.

Powder coatings improved as exhibited by SEM/ EDS of SiC with a TiN barrier coating covered with a Cu overlayer (Figs 8 and 9). Sample Bl showed good coverage, though not perfect, and was markedly improved with more than 95% of the SiC grains exhibiting uniform coverage with a Ti and Cu rich coating (Fig. 8). Note that the Si and the Ti EDS peaks from the TiN coated SiC powders were

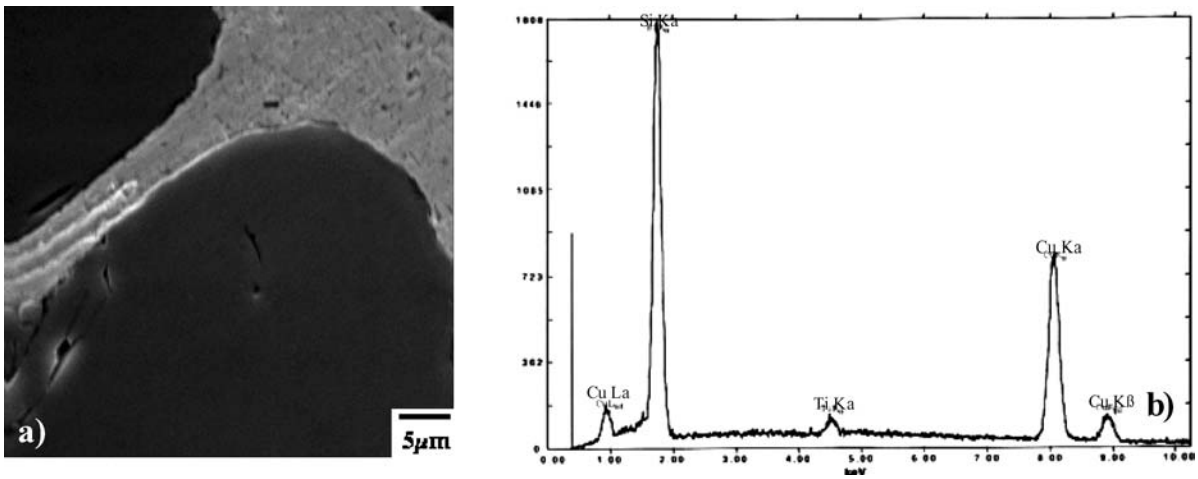

Figure 12 (a) SEM image of sample HD showing the angular morphology of the SiC grains and intermittent Ti coating, (b) EDX spectrum.

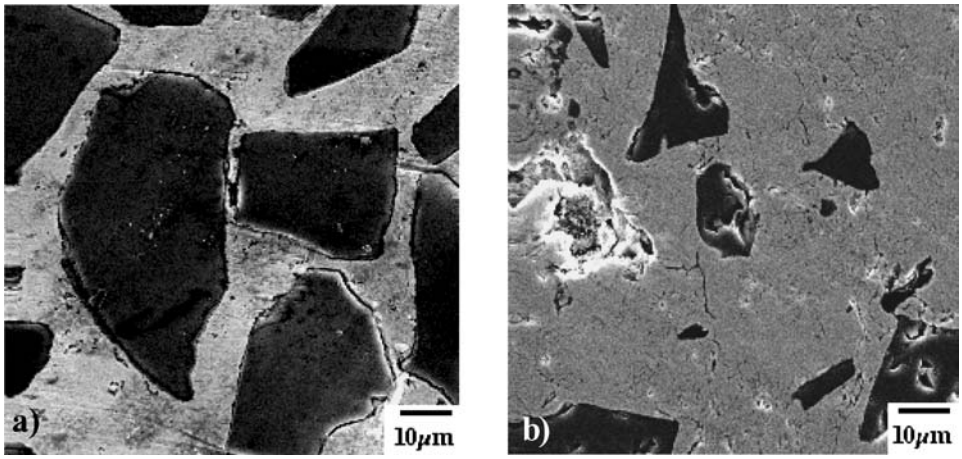

Figure 13 (a) SEM image of Sample HE showing imperfect densification, (b) SEM image of HF showing microporosity and striations.

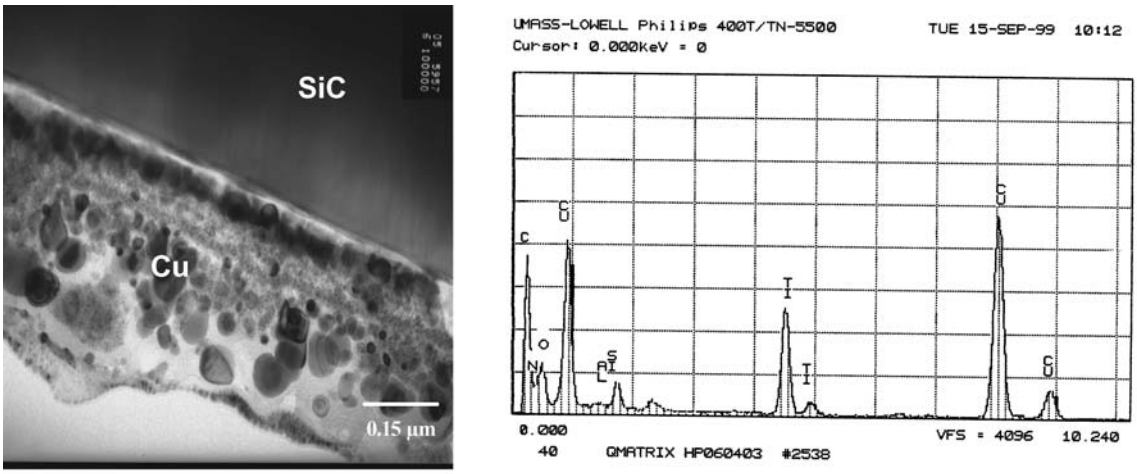

Figure 14 TEM/EDS of Cu/SiC interface sample HD exhibiting impurities for 50 vol% Cu: 50 vol% SiC after hot pressing at 910°C for 40 min at 7.7 ksi.

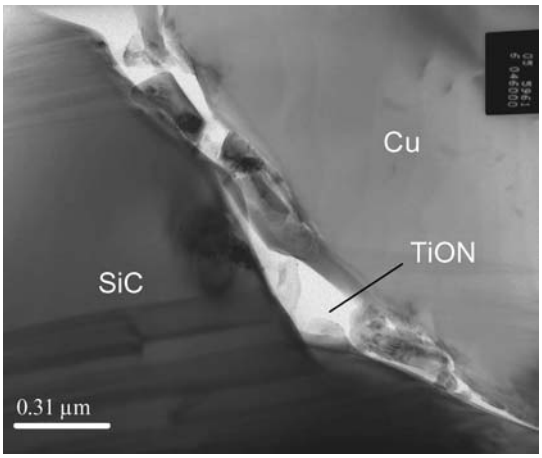

Figure 15 TEM of Cu/SiC interface for 50 vol% Cu: 50 vol% SiC sample HD after hot pressing at 910°C for 40 min at 7.7 ksi.

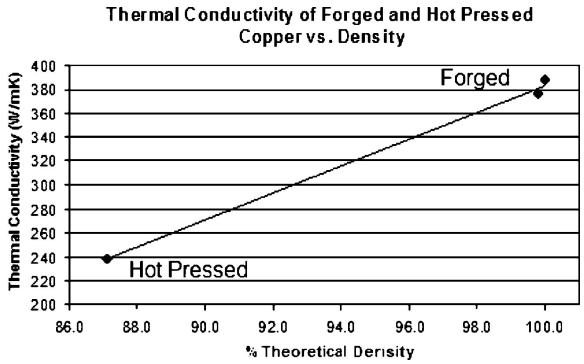

Figure 16 Thermal conductivity of forged and hot pressed high purity Cu as a function of density.

suppressed due to the absorption of those characteristic X-rays by the Cu over-layer (Fig. 8c). Fig. 8d is the TEM image of the coated SiC powder showing separation of the Cu grains from the SiC. The sample preparation for TEM imaging entailed a rigorous abrasive thinning causing the coating to be partially removed from the SiC powder. The stress placed upon the coating for TEM specimen preparation was considered to be far in excess of that experienced by a powder during pressure densification. Consequently, although this powder was not optimal, it was deemed to be of sufficient quality to be used for hot pressing.

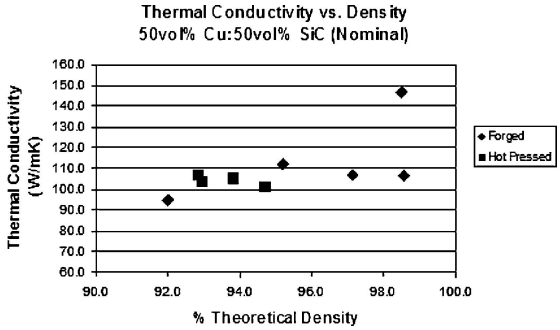

Figure 17 Thermal conductivity as a function of density for hot pressed and forged 50 vol% Cu: 50 vol% SiC.

Unlike prior coatings on SiC powders, sample B2 was an excellent coated powder with complete coverage of over 97% of the SiC grains. Fig. 9a shows an excellent coating with only the Cu over layers detected with EDS analysis (Fig. 9b). The coatings were more adherent and withstood the rigors of TEM sample preparation to allow analysis of the TiN coating in-situ on the SiC powder (Fig. 9). The barrier coating was Ti based with a significant amount of both oxygen and nitrogen, and is likely a titanium oxynitride (Ti–O–N). The barrier coating was ~50 nm thick, target coating thickness was 70 nm.

TABLE V Density and thermal conductivity of 50 vol% Cu: 50 vol%SiC (Sample HA) after hot pressing for 40 min at 7.7 ksi

Hot press temperature (°C)	Density (gm/cm)	% Theoretical density	Thermal conductivity (W/mK)
1065	5.941	92.8	107.0
1006	5.951	93.0	104.0
953	6.007	93.8	105.2
910	6.069	94.7	101.2

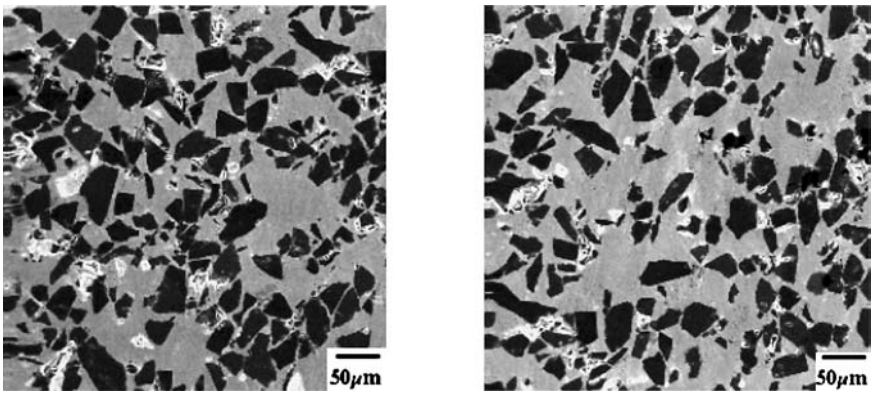

Figure 18 SEM micrograph of cross-sectioned, fully dense, forged CuSiC sample FA.

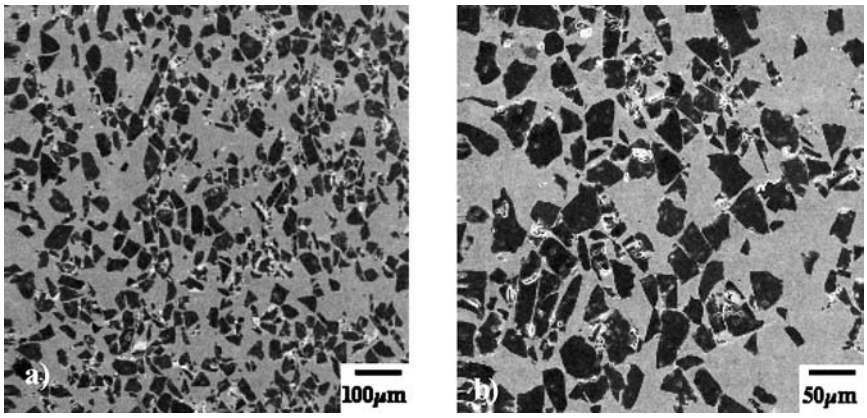

Figure 19 SEM micrographs of sample FB after forging (Cu blended with Cu/TiN coated SiC).

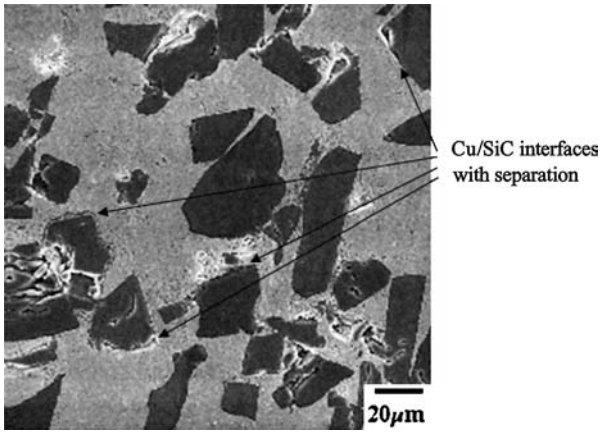

Figure 20 SEM micrographs of sample FA after forging showing interfaces with separation.

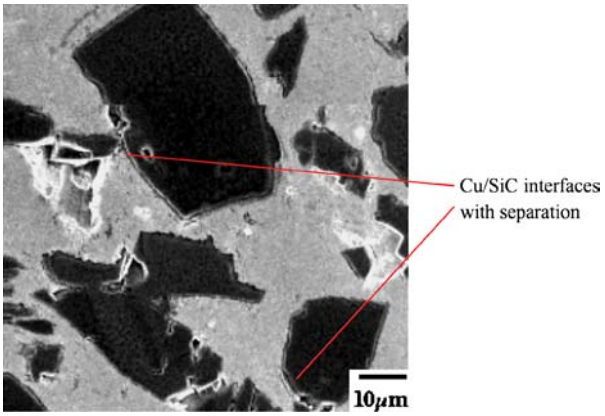

Figure 21 SEM image of sample FC after forging showing interfacial separation.

3.1.2. Characterization of hot pressed CuSiC composites

The major problem facing the hot pressing of CuSiC composites was to achieve complete densification. The blending of additional Cu into the Cu/TiN coated SiC prior to hot pressing was an attempt to provide sufficient Cu to fill all of the intergranular pores after hot pressing and to achieve full densification without appreciable porosity.

High purity Cu powder (99.74 wt% pure), D2 was blended into the Cu/TiN coated SiC to increase the nominal 19 vol% Cu to a final body of 40 vol%Cu: 60 vol% SiC. A 40 vol% Cu: 60 vol% SiC hot pressed coupon achieved a density of 4.79 gm/cm^3 (87% of theoretical density) after hot pressing to 1054°C at a pressure of 4.7 ksi after a 40 min soak. An additional 40 vol% Cu: 60 vol% SiC blend resulted in a density of 4.81 gm/cm^3 (88% of theoretical density) after hot pressing at 1065°C at 5.9 ksi after a 40 min soak.

TABLE VI Chemical analysis by GDMS, ICP and LECO Combustion for 50 vol% Cu: 50 vol% SiC hot pressed for 40 min at 7.7 ksi

Hot press temperature (°C)	Cu (wt%)	Total Cu (vol%)	SiC (vol%)	Impurities (wt%)	Oxygen (wt%)	Si dissolved in Cu (ppmw on total body basis)
910	77.9	56.0	44.0	0.09	0.33	<39
1065	77.8	55.8	44.2	0.09	0.35	<39

About 95% of theoretical maximum density (Table V) was achieved by increasing the content of the plastically deformable Cu component to 50 vol% Cu: 50 vol% SiC and increasing pressure to 7.7 ksi for the next hot press trials. However, quite surprisingly thermal conductivity calculated from thermal diffusivity measurement was very low, between 101.2 and 107.0 W/mK. This may be due to the following

- Interfacial reactions occurring as a consequence of poor barrier coatings or
- Microporosity present in the Cu as elongated striations that did not completely weld together or
- Impurities present in the powders prior to hot pressing that resulted in such low thermal conductivity values.

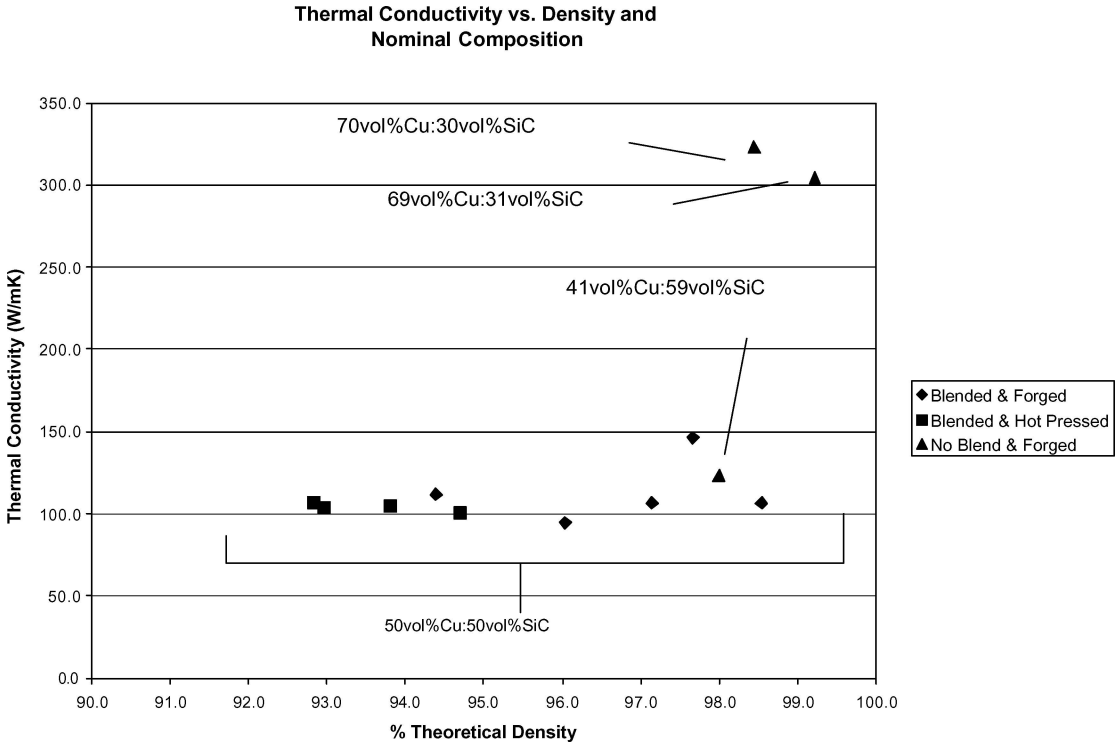

Figure 22 Thermal conductivity versus density and composition for forged CuSiC.

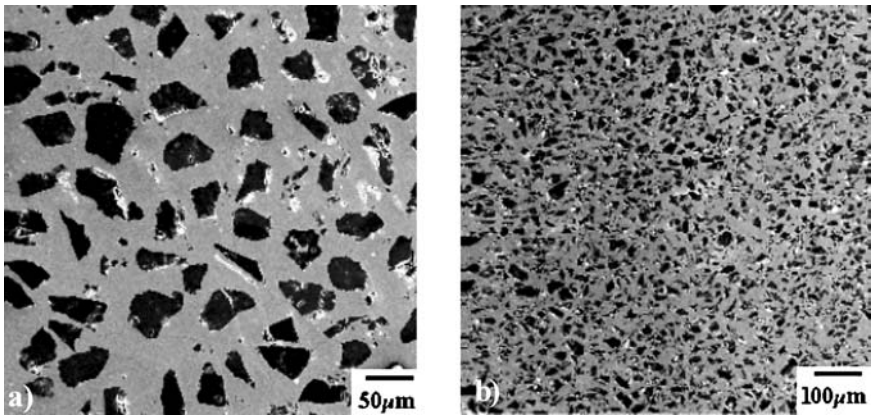

Figure 23 SEM micrograph of: (a) sample FF and (b) sample FD. Both samples were made with all Cu directly deposited on SiC.

TEM micrographs of cross-sectioned CuSiC composite (Sample HF) after hot pressing at 1065°C for 40 min at 7.7 ksi show variable thickness of the TiN barrier at the Cu/SiC interface (Fig. l0a, c and e). There was an intermittent Ti presence at the Cu/SiC interface as determined by TEM/EDS. There were no crystalline products of reaction at the Cu/SiC interface for the hot pressed Cu/TiN coated SiC powders that were detected earlier by TEM electron diffraction for uncoated α-SiC rods after immersion in liquid copper. In sample HE, the angular morphology of the SiC grains was preserved after hot pressing which was supportive of no reaction between Cu and SiC (Fig. 11). SEM images of the cross-sectioned Cu/TiN coated SiC composite, sample HD after hot pressing at 910°C for 40 min at 7.7 ksi detected an intermittent Ti presence at the Cu/SiC interface for some of the grains (Fig. 12). Again, the angular morphology of the SiC grains were retained and considered supportive of minimal or no reaction between the Cu and SiC.

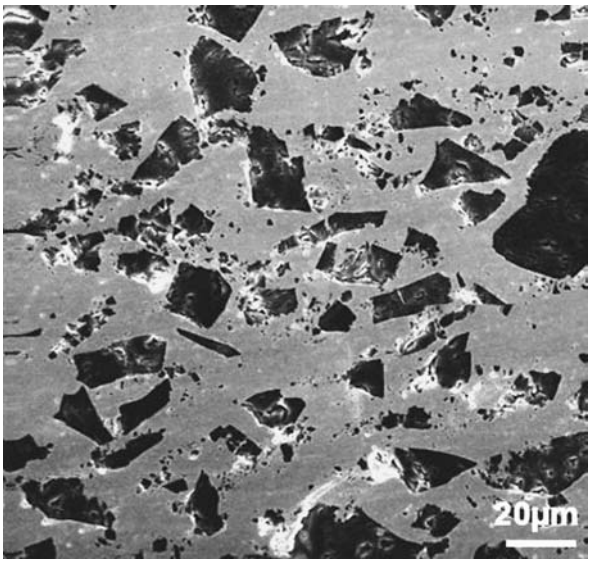

Figure 24 SEM micrographs of sample FD made with all Cu directly deposited on SiC.

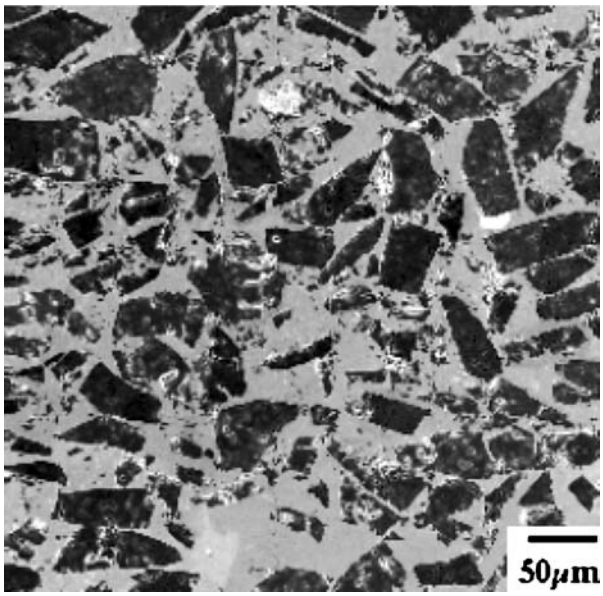

Figure 25 SEM micrograph of the sample FG.

There was no evidence to support sufficient interfacial reaction to result in a 62% decrease in the expected thermal conductivity values. Hence interfacial reactions may not be the primary cause for such low thermal conductivity values and that microporosity and impurities might have played a more significant role. Fig. 13 shows a large number of striations and pores that indicated incomplete densification in samples HE and HF. This may be the primary contributor to the low thermal conductivities obtained from hot pressed composites.

The presence of impurities was a concern since this may have been a secondary effect in the decrease of thermal conductivity of the hot pressed CuSiC body. Appreciable amounts of Al and O were detected at the Cu/SiC interface and Ti was conspicuously absent for the sample HF after hot pressing at 1065°C for 40 min at 7.7 ksi (Fig. 10).

The presence of Al and O impurities was also detected by TEM/EDS at the Cu/SiC interface after hot pressing at 910°C for 40 min at 7.7 ksi (Fig. 14). Spectra from Si, C and Cu were expected and would be consistent with the presence of SiC and Cu. TEM elemental analysis detected both Ti and N after the 910°C hot press of sample HD, whereas these elements were intermittently detected after the 1065°C hot press of sample HF. Possible degradation of the thin TiN barrier in contact with the Cu may have occurred at the 1065°C hot press temperature. This may explain the increase in Ti concentration from l000 to 2100 ppmw as detected by ICP analysis of the nitric acid soluble, Cu portion of the CuSiC bodies hot pressed at 910°C and 1065°C, respectively.

Additional analysis of the Cu/SiC interface at higher magnification revealed Ti with the concomitant presence of O and N. The barrier coating is likely to be a form of titanium oxynitride (Ti–O–N) and not pure TiN (Fig. 15).

Chemical analysis of the Cu/TiN coated SiC powder blended with high purity Cu to 50 vol% Cu: 50 vol% SiC after hot pressing is summarized in Table VI. Silicon dissolved in Cu and all other elemental concentrations of Table VI are reported on a total body basis as opposed to a fraction of the dissolved solids.

TABLE VII Thermal conductivity of the forged composites versus percent theoretical density

Sample	% Theoretical density	Thermal conductivity (W/mK)
FA	96.0	94.6
FB	98.5	106.4
FC	97.1	106.8
FD	99.2	304.5
FE	94.4	111.9
FF	98.4	322.9
FG	98.0	123.3

The total impurities were low, ~0.1 wt% on metals basis with 0.33 to 0.35 wt% O. However, it is known that small amounts of Si can degrade Cu thermal conductivity. Also, the presence of O can oxidize Cu causing a decrease in plasticity and possibly impede densification. These concerns were addressed as a precaution in the next round of pressure densification trials by the use of powders of higher purity for forging.

3.2. Characterization of forged CuSiC composites

The goal of the forging study was to eliminate porosity while insuring minimal Cu/SiC reaction by using higher compressive and shear stress at lower temperature and shorter time. Forging of high purity Cu alone at 850°C and 50 ksi was more successful than hot pressing between 910 and 1065°C at 7.7 ksi to achieve full density. The direct relationship between thermal conductivity and porosity is demonstrated in Fig. 16. Forged Cu coupons achieved thermal conductivity of +380 W/mK when porosity was eliminated (Fig. 16).

Initially, forged coupons were forged from Cu/TiN coated SiC powders blended with high purity Cu to make a 50 vol% Cu: 50 vol% SiC material. The post-forged density and thermal conductivity were between 94.4 to 98.5% theoretical density and 94.6 to 146.5 W/mK. The thermal conductivity was lower than predicted in part due to porosity and incomplete densification.

It is difficult to predict thermal conductivity for a Cu-SiC two phase system since heat transfer is dependent upon size and distribution of the SiC phase within the continuous Cu phase, as well as the nature of the interface between each phase. A rough estimate of thermal

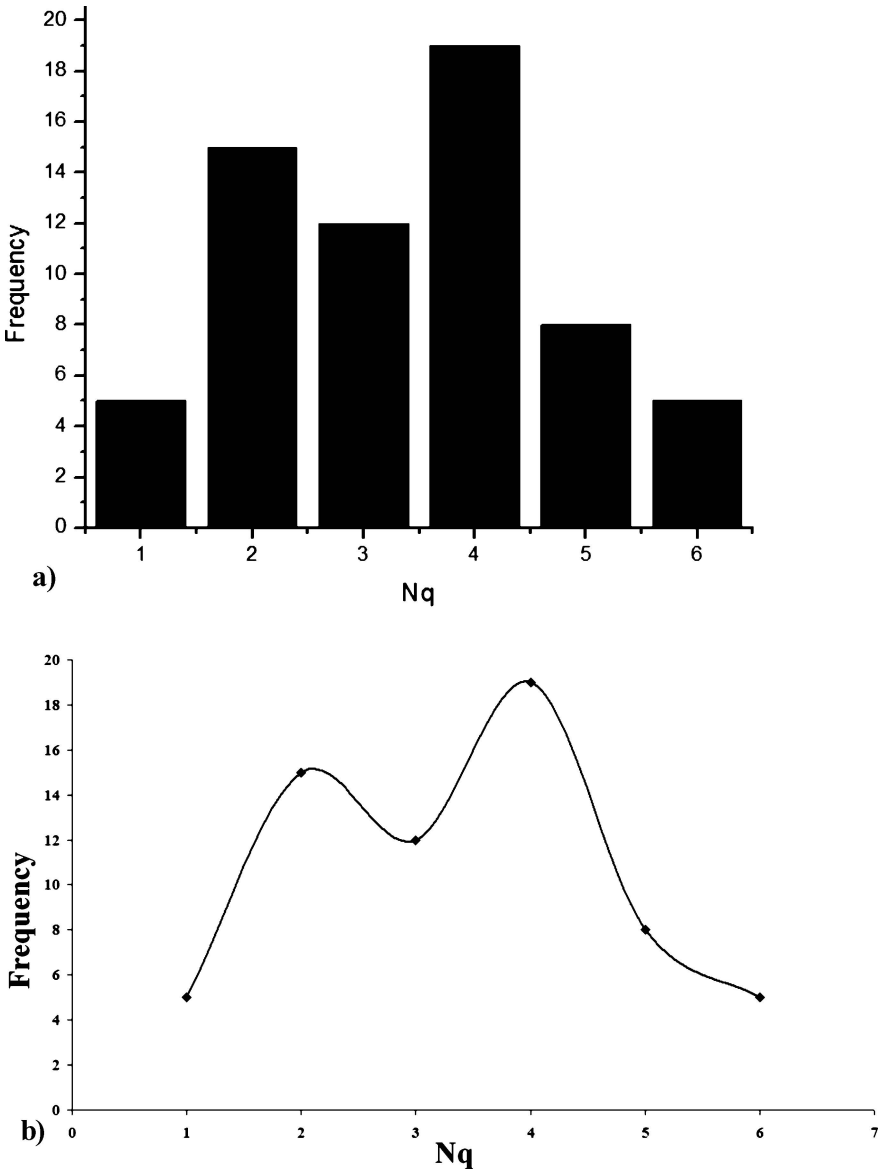

Figure 26 SiC grain distribution of sample FD: (a) Frequency histogram, and (b) frequency vs. N_q distribution curve.

conductivity of 282 W/mK was calculated using the rule of mixtures for 50 vol% Cu: 50 vol% SiC. It was unexpected to see thermal conductivity of 146.5 W/mK and lower for a CuSiC body within 1.5% of theoretical density. Note that although thermal conductivity did decline with decreasing density for high purity Cu (without SiC), the thermal conductivity decreased by 36% with a 13% decrease in density (Fig. 16). The CuSiC body with the greatest forge density experienced a 62% decrease from the estimated maximum thermal conductivity with only a 1.5% decrease in density from theoretical, complete density (Fig. 17). This was surprising and suggested that porosity alone was not the sole determinant of the low thermal conductivity of the forged materials.

It was visually observed after blending of Cu and SiC powders before forging that segregation of Cu and SiC occurred. Segregation of Cu and SiC was not entirely unexpected since the density of individual Cu and SiC powder grains were dissimilar at 8.92 and 3.217 gm/cm^3, respectively. Segregation for the blended compositions was visually observed after forging, also. Micrographs of the SiC distribution in forged coupons show imperfect distribution of the SiC grains inside the continuous Cu matrix (Figs 18 and 19).

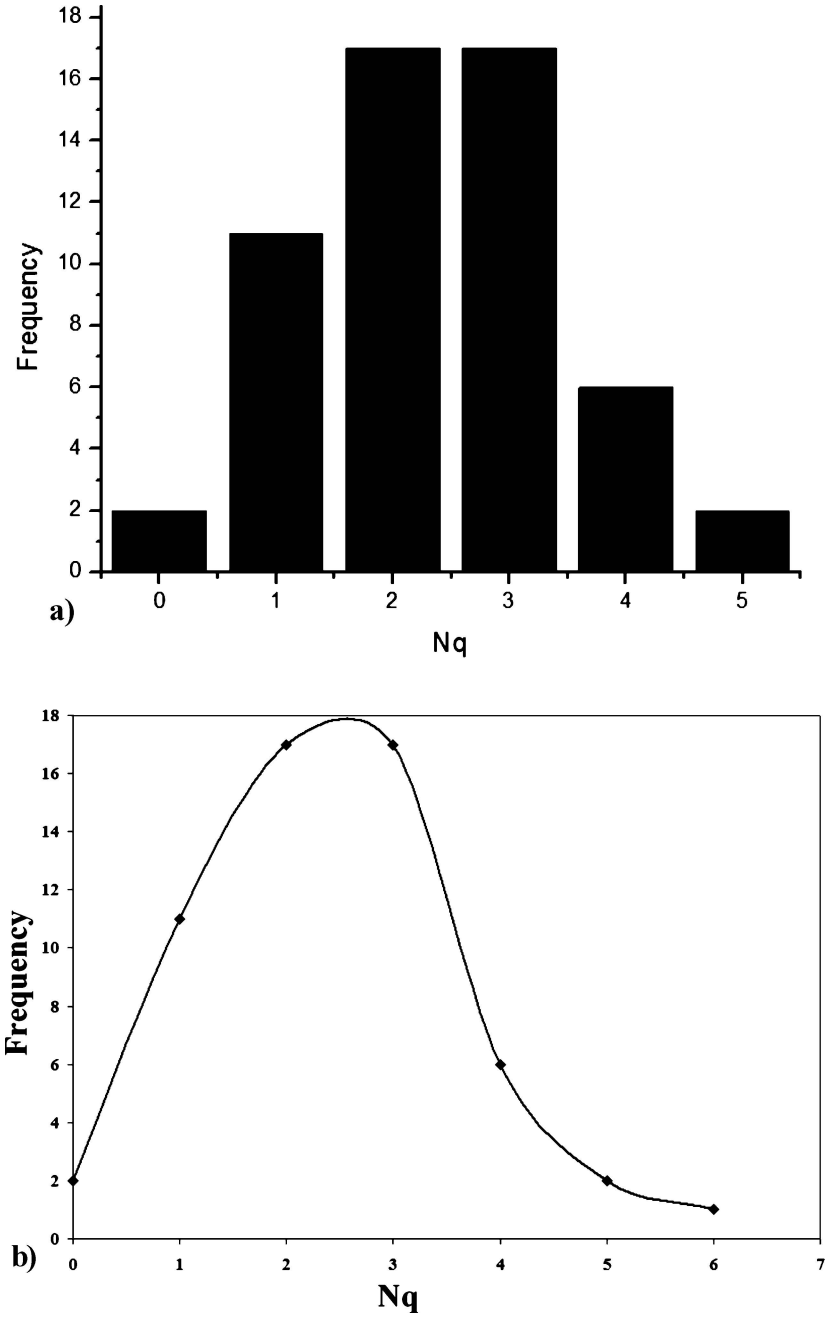

Figure 27 SiC grain distribution of sample FB: (a) frequency histogram, and (b) frequency vs. N_q distribution curve.

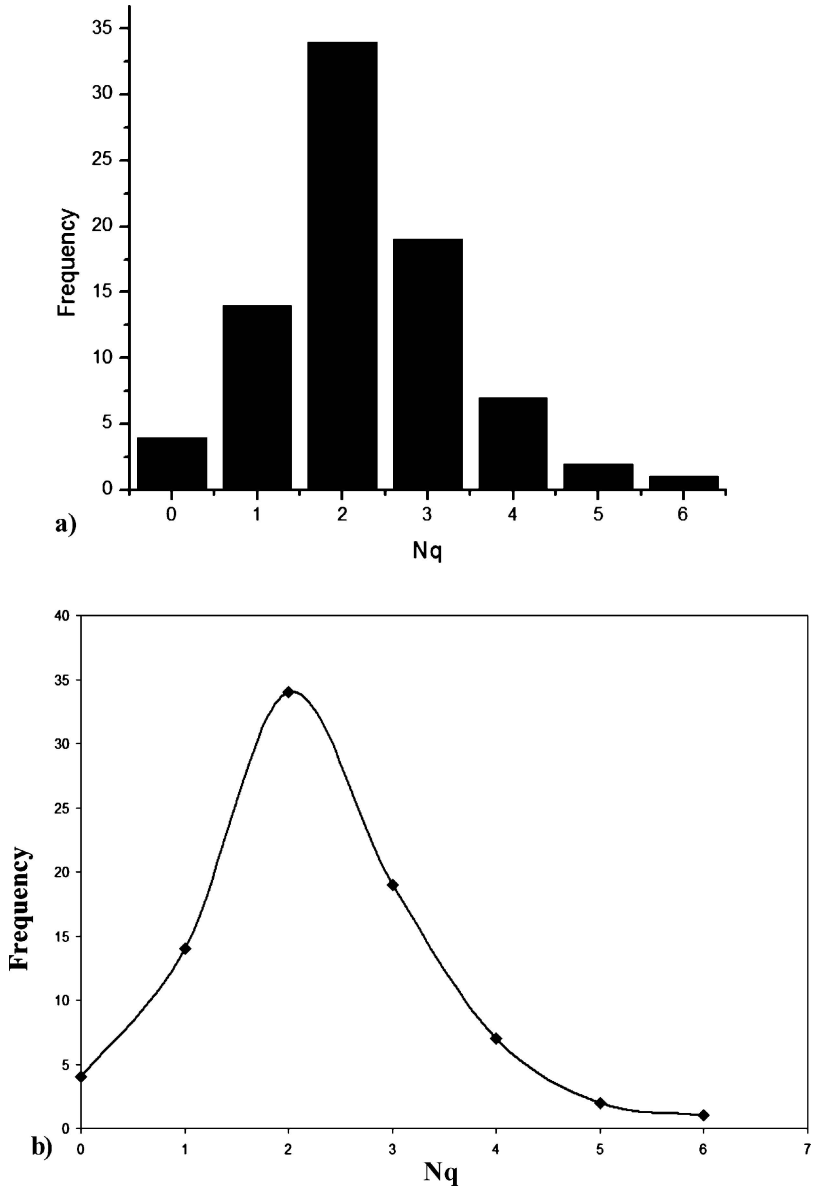

Figure 28 SiC grain distribution of sample FC: (a) frequency histogram, and (b) frequency vs. N_q distribution curve.

Regions with more SiC and a deficit of Cu will likely be more difficult to densify since Cu alone plastically deforms during consolidation to flow around SiC grains. The flow of Cu around a localized region of densely packed SiC grains will be impeded by the SiC obstructions in the Cu flow path. Minimizing Cu and SiC segregation to insure more uniform SiC distribution should be beneficial to assist densification. Also, local increases of SiC concentration will create more Cu/SiC interfaces with an expected increase of the interfacial thermal resistance to impede heat transfer.

Forged CuSiC, sample FA made from blended powders also showed some separation between the Cu and SiC grains (Fig. 20). This feature was also identified in sample FC (Fig. 21). This feature could be due to elastic spring-back of the Cu after forge pressure was removed. Poor contact between Cu and SiC grains was expected to impede heat transfer.

The forged samples FD, FF and FG were made by coating all of the Cu needed to make the CuSiC body directly onto the SiC powder to eliminate blending and associated segregation. This led to desired results with the samples FD and FF being the only formulations that achieved theoretical density as well as high thermal conductivity of 304.5 and 322.9 W/mK, respectively (Fig. 22). It must also be noted that these formulations had higher Cu content than prior formulations (69 vol% Cu: 31 vol% SiC and 70 vol% Cu: 30 vol% SiC respectively).

The distribution of SiC grains within the Cu matrix was most uniform for forged CuSiC made by coating all of the Cu directly onto the SiC (Fig. 23). This eliminated Cu and SiC segregation effects that resulted from blending powders. Higher magnification SEM

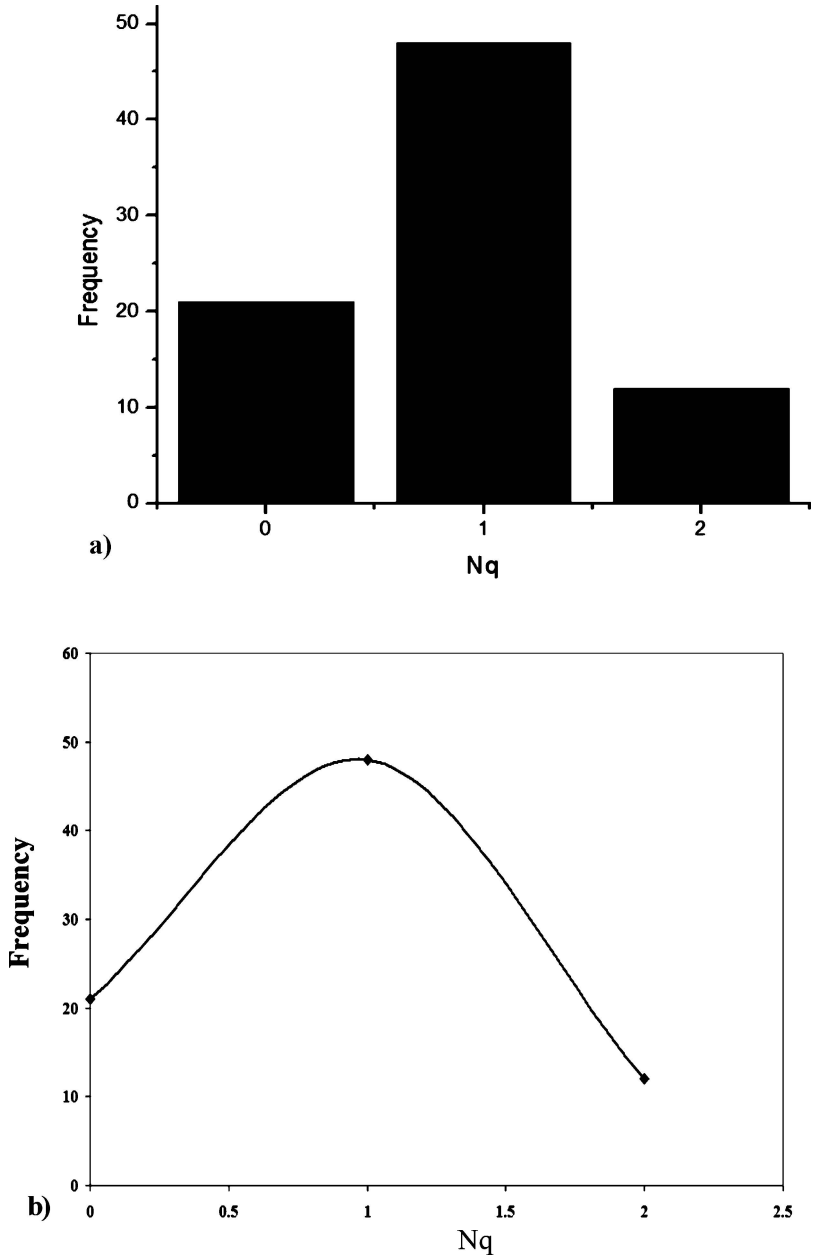

Figure 29 SiC grain distribution of sample FF: (a) frequency histogram, and (b) frequency vs. N_q distribution curve.

micrographs (Fig. 24) also show the absence of porosity and good contact between SiC grains and surrounding Cu matrix.

From Fig. 22, it was concluded that the deposition of Cu directly onto the coated powders had a positive impact on thermal conductivity primarily because it reduced segregation and promotes a more uniform distribution of the SiC grains in the Cu matrix. It was interesting to note that the forged sample FG which also had Cu deposited directly on the SiC grains prior to forging had poor thermal conductivity values despite having 98% theoretical density. This was in part due to its high SiC composition of 41 vol% Cu: 59 vol% SiC which resulted in a clustered distribution of the SiC grains in the Cu matrix (Fig. 25).

It was surmised that the uniformity of the particle distribution played an important role in attaining good thermal conductivities. Variability of SiC grain distribution uniformity may explain the variable thermal conductivity for forged samples of equivalent high density (Fig. 22, Table VII). The following section investigated the relationship of SiC grain distribution with the thermal conductivity of the composites.

3.3. Particle distribution measurements

3.3.1. Quadrat method

Quadrat analysis of the SiC grain distribution of forged CuSiC was used to determine the uniformity of the SiC distribution in the Cu matrix. Analyses of the CuSiC samples (Table IV and Fig. 5) are given as frequency

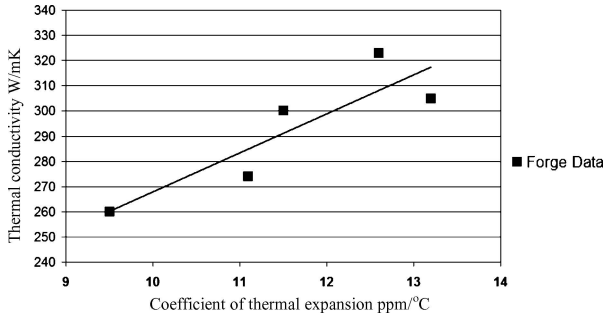

Figure 30 Thermal conductivity vs. CTE measurements from 25 to 150°C for forged CuSiC.

histograms of the number of SiC particles per quadrat, N_q. The N_q distribution curve (Fig. 26b) of the sample FD was symmetric and appeared to follow the binomial model of distribution which represented a regular spatial distribution of points (Fig. 4) [13]. The distribution had a mean of ∼3.4 particles per quadrat with a standard deviation of 1.37. It can be inferred from the frequency histogram that ∼69% of the quadrats had 3 or more particles which indicated uniform distribution of SiC particles (Fig. 26a).

The N_q distribution curve appeared to be similar to the Poisson distribution curve of the FB forged specimen suggesting a random spatial distribution (Fig. 27b). The distribution had a mean N_q of ∼2.5 particles per quadrat with a standard deviation s of 1.22. The N_q histogram showed that approximately 84% of the quadrats have three and less particles, a strong indication of clustering and demonstrative of significant deviation from uniform particle size distribution.

Sample FC forge had an N_q distribution curve (Fig. 28b) similar to the Poisson distribution curve again suggesting a random spatial distribution as sample FB. The distribution had a mean N_q of ∼2.25 particles per quadrat with a standard deviation s of 1.14. Fig. 28a shows 64% of the quadrats had two and less particles which indicated clustering. Sample FF had the best distribution curve (Fig. 29b) which closely resembled the nominal distribution curve of a regular spatial distribution. This was a highly uniform and a near perfect example of the desired, regular SiC grain distribution.

3.3.2. Skewness of the N_q distribution

An effective method of characterizing the distribution of particles in a matrix was to calculate the skewness of the data which was the degree of asymmetry around the mean N_q [13]. It was determined from the literature that the smaller value of ß corresponds with less clustering and better uniformity of the distribution. Sample FF had the least skewness value (Table VIII), an indicator of the most uniform distribution followed in turn by samples FD, FB and FC with increasing skewness. Sample FC had the highest skewness value which indicated a greater degree of clustering than the other samples. These results further substantiated the micro structural observation which suggested that Sample FF and FD as the most uniformly distributed composites.

TABLE VIII Skewness measurement of the composites

CuSiC sample	Skewness 6
FF	0.085
FD	0.11
FB	0.45
FC	0.55

4. Conclusions

Hot pressing Cu blended with Cu/TiN coated SiC powder achieved only 94.7% of theoretical density with a maximum thermal conductivity of 107 W/mK. Micro-porosity was believed to be the primary cause for poor thermal conductivity. Forging improved densification, but it was believed that densification was impeded by Cu-SiC segregation during blending which affected SiC distribution during and after densification. Segregation was eliminated by coating all of the Cu directly onto SiC. Complete densification (+99% of theoretical) was achieved with corresponding thermal conductivity of 322.9 W/mK. The particle distribution was also influenced by grain size. Samples FD and FF were processed with powders with a nominal 325 mesh size and had a uniform distribution as compared to samples FB and FC processed with powders of nominal 240 mesh size. Forging was successful to decrease thermal exposure of Cu and SiC to manufacture CuSiC MMC with 322.9 W/mK thermal conductivity and CTE at 21°C of 11 pppm/°C (Fig. 30). The practical CuSiC range of thermal conductivity is expected to be from 260 to 320 W/mK with coefficient of thermal expansion between 8.5 and 12.0 ppm/°C, respectively.

Future work will investigate both melt processed and forged CuSiC MMC with higher SiC volume fraction. Experience with similar particle reinforced MMC material systems strongly suggests that fully dense CuSiC MMC baseplates with CTE of 9 ppm/°C and 270 W/mK will be possible by forging.

References

1. G. J. SUNDBERG *et al.*, Proceedings of PCIM 2001 Power Electronics Conference, Rosemont September (2001) p. 172.
2. N. J. GERNERT *et al.*, Thermacore International, www.thermacore.com/pdfs/kilowatt.pdf, p. 1.
3. C. RADO, B. DREVET and N. EUSTATHOPOULOS, *Acta Materialia* **48** (2000) 4483.
4. E. KOLAWA, J. S. CHEN, J. S. REID, P. J. POKELA and M. A. NICOLET, *J. Appl. Phys.* **70** (1991) 1369.
5. C. RADO, S. KALOGEROPOULOU and N. EUSTATHOPOULOS, *Scripta. Mater.* **42** (2000) 203.
6. D. TYLER and W. BLACK, www.asminternational.org/hbo/do/highlight/content/V02/D01/A09
7. J. J. LEWANDOWSKI, C. LIU and W. H. HUNT, *Mater. Sci. Eng.* A**107** (1989) 241.

8. L. C. STONE and P. TSAKIROPOULOS, *Mater. Sci. Technol.* **11** (1995) 213.
9. W. A. SPITZIG, J. F. KELLY and O. RICHMOND, *Metallography* **18** (1985) 235.
10. H. SCHWARZ and H. E. EXNER, *J. Microsc.* **129** (1983) 155.
11. K. H. HANISCH and D. STOYAN, *ibid.* **122** (1981) 131.
12. A. OLSZOWKA-MYALSKA, J. SZALA and J. CWAJNA, *Mater. Characterization* **46** (2001) 189.
13. P. A. KARNEZIS, G. DURRANT and B. CANTOR, *ibid.* **40** (1998) 97.
14. R. T. DEHOFF and F. N. RHINES, "Quantitative Microscopy" (McGraw-Hill, New York, 1968).
15. E. E. UNDERWOOD, "Quantitative Stereology" (Addison-Wesley, Reading, MA, 1970).
16. I. SAXL, Distance methods in metallurgy. Proc IV Int Conf STERMAT'94, WislCa (October 3–6). Fotobit Design, Krakow, Poland, p. 65.
17. L. M. KARLSSON, Proc IV Int. Conf STERMAT'94, WislCa (October 3–6). Fotobit Design, Krakow, Poland, p. 249.
18. J. CWAJNA, A. OLSZOWKA-MYALSKA, J. SZALA, *Acta Stereol.* **11** (1992) 431.
19. A. ROGERS, "Statistical Analysis of Spatial Dispersions" (The Quadrat Method. Pion, London, 1974).
20. K. J. KURZYDLOWSKI and B. RALPH, "The Quantitative Description of the Micro Structure of Materials" (CRC Press, Boca Raton, FL, 1995).
21. P. GREIG-SMITH, *Ann. Bot.* **16** (1952) 293.
22. J. T. CURTIS and R. P. MCLNTOSH, *Ecology* **31** (1950) 434.

Received 8 December 2004
and accepted 27 May 2005